University of Baghdad
College of Engineering
JOURNAL OF ENGINEERING

Journal of Engineering

journal homepage: www.jcoeng.edu.iq

Volume 31 Number 1 January 2025

Envelope of Collapse in Gypseous Sandy Soils using Finite Element Method and Particle Image Velocimetry

Hala Mahmood Jawad [1], **Zuhair Kadhim Jahanger** [2,*]

[1]Department of Civil Engineering, College of Engineering, University of Baghdad, Baghdad, Iraq
[2] Department of Water Resources Engineering, College of Engineering, University of Baghdad, Baghdad, Iraq

ABSTRACT

Water level rise as well as inundation to gypseous soil medium can lead to a substantial loss of volume of the soil, with or without adding load. Macromechanical behavior of gypseous sandy soils using particle image velocimetry (PIV) is yet to be studied, with a particular emphasis on patterns of collapse. These unique patterns have given attention to researchers on deformable soils, but the difficulties of gypseous sandy soil still need to be addressed. Consequently, this study aims to quantify the local-scale displacement fields and patterns of failure of gypseous sand interacting with rigid strip foundations under static stress under comparison, emphasizing wetting due to rising the water table and the dry state using an experimental model and finite element method (FEM). The PIV results showed that the pattern of collapse of the gypseous sandy soil is of the type of punching shear failure, which validated the FEM and these patterns related to soil vertical deformation. Where FEM and PIV results were corresponded well. In addition, the built soil models in FEM are essentially oversimplified representations of the real behavior of the foundation. The outcomes reveal that local scale failure patterns of gypseous soil medium are essential for improving the design of foundations.

Keywords: Gypseous soil, Strip footing, Collapse pattern, Particle image velocimetry (PIV), Finite element method (FEM).

1. INTRODUCTION

A foundation is the lowest part of a structure which transfers the impose load to the underneath soil. There are many types of foundations such as shallow and deep foundations **(Das, 2017)**. Shallow foundations, such as individual and strip footings, are typically described as square or rectangular, where individual footings support columns, while strip footings are used to support walls or either column **(Zedan and Abbas, 2020)**. To design the foundation of a structure, an engineer must comprehend the soil deposit types that support the foundation **(Vaughan, 2009)** using field and laboratory tests. There are

*Corresponding author
Peer review under the responsibility of University of Baghdad.
https://doi.org/10.31026/j.eng.2025.01.08

Article received: 26/04/2024
Article revised: 19/08/2024
Article accepted: 12/10/2024
Article published: 01/01/2025

numerous soil types, and one of these is gypseous, which is calcium sulfate, which is created when sediments in dry and semi-dry regions with brine are heated and pressured **(Punmia and Jain, 2005).** Problematic soil typically contains significant amounts of gypsum, and gypsum is considered a mineral salt represented by Hydrated Calcium Sulphate ($CaSO_4 \cdot 2H_2O$) to impact its behavior and is referred to as gypseous soil **(Mohsen and Albusoda, 2022; Hassan and Al-Busoda, 2023)**. Furthermore, gypseous soil is classified as collapse soil, where soil contains was different percentages content of gypsum, especially in Iraq and other countries **(Ahmad et al., 2012)**. When geotechnical and geological engineers are tasked with identifying collapsing soils, estimating the degree and extent of future wetness, determining the collapse potential, and selecting a design or mitigation option, the uncertainty in predicting future wetness and the typically high degree of non-homogeneity of soil profiles in arid regions increase the difficulty of collapsible soil studies. Collapse potential is most significantly exacerbated when the existence and magnitude of the potential fail to be identified before construction. As a result, to design appropriately for these moisture-sensitive soil sites, it is necessary to identify collapsible soils and evaluate their potential for collapse **(Abd-Alhameed and Al-Busoda, 2023)**.

To forecast potential foundation settlements, it is customary to perform quantitative or laboratory assessments of collapse potential **(AbdulRahman et al., 2021)**. Hence, through the utilization of PIV for the examination of gypseous soil behavior, engineers will acquire enhanced capabilities to overcome the obstacles that arise in Iraq and other similar locations. Due to the global prevalence of gypseous soils, it is vital to research this subject in Iraq. The distinctive properties exhibited by gypseous soils have garnered considerable attention from investigators. The strength and rigidity of these soils are significantly diminished upon exposure to water **(Al-Saoudi et al., 2013)**. In case gypseous soil-based structures to collapse, it is critical to comprehend the behavior of these soil in a variety of environments. The impact of gypsum dissolution on the mechanical properties of gypseous soils in Iraq was investigated **(Al-Mufty, 1997)**. Furthermore, further research employing both laboratory and field techniques appears to be necessary to gain a comprehensive understanding of the behavior of gypseous soils, which **(Al-Saoudi et al., 2013)** have identified as a significant obstacle in Iraq. Another study that investigated the topic of gypsiferous soils in Iraq **(Kuttah and Sato, 2015)** explored potential solutions to this problem. Analyzing the settling of gypseous sand subsequent to a brief wet period used oedometer test **(Husain et al., 2018)**. The investigation unveiled that soil deformation exhibited spatial variability, with notable alterations occurring exclusively in designated areas. Therefore, more sophisticated methodologies, such as Finite Element Method and PIV, should be utilized to investigate the behavior of collapsible soils.

The analysis of soil deformation patterns was conducted using particle image velocimetry (PIV) **(Adrian, 1991)**. Particle image velocimetry is an optical method that can be used to ascertain the velocity fields of solids and fluids. PIV captures images of particles in a fluid or solid using a high-speed camera and a laser sheet to illuminate the particles. The photographs are subsequently subjected to advanced algorithms to extract velocity fields. The program PIV incorporates numerous disciplines, including fluid mechanics and soil mechanics, these are two to understand the behavior of fluids and solids better. In recent years, PIV has been widely applied to investigate the response of soils to a variety of stresses. **(Alimardani Lavasan and Ghazavi, 2014)** investigated the soil pattern deformation and the mechanism of failure utilized beneath interfering square foundations employing PIV. **(Adrian, 1991)**, on the other hand, utilized PIV to analyze fluid flow around submerged barriers and found it to be an exceptional instrument for elucidating soil behavior in diverse

scenarios. Furthermore, an investigation was carried out using comparative PIV to characteristics of grain-structure interactions focused on the sand medium of different packing densities **(Jahanger et al., 2018b)**. By employing PIV and other methodologies, engineers can therefore devise practical solutions to mitigate the deleterious effects of gypseous soils through enhanced comprehension of their behavior.

Gypseous soils face many challenges in terms of significant loss of shear strength and volume when exposed to water, such as rain, and irrigation, which is attributed to increased groundwater capillaries. Therefore, civil engineers must take into account factors related to soil bearing capacity when designing structures or foundations on the soil itself. In addition, numerous bearing capacities and soil displacements have been found in literature. These tests demonstrate the correlation between shear strength, compressibility, settlement, and soil carrying capacity for different soils. These analyses also highlighted the significance of thinking about how soil movement may affect building substructures **(Al-Obaidi et al., 2022)**. They used geotextile reinforcement to investigate the bearing capacity and collapse susceptibility of gypseous soil. It was determined that the impacts of soil movement were significant. Sometimes the dynamics of stressed soil may be seen using PIV. However, there are currently insufficient tests that demonstrate how gypseous sandy soils interact with foundations, like strip and square footing constructions, in terms of total displacement diagrams (failure envelope). Consequently, the precise measure of soil deformation is typically unattainable during field tests, as such assessments solely evaluate the footing pressure and settlement. When the stress-settlement relationships for the single collapsible soil odometer test are compared to those for sandy soil, it is clear that the behavior of the gypseous sandy soil (collapsible soil) being tested is very different. When the same amount of stress was put on the surface foundations during the experiment, the local-scale displacement fields should have shown these differences as well. Because of this poor knowledge of soil gypseous deformations and internal shearing mechanisms, there are problems verifying engineering computations.

The failure mechanisms and kinematic behaviors of gypseous sand deposits subjected to shallow footings under vertical static pressures are not well described by the experimental data that are currently available. Studying the interactions between medium-dense gypseous sand (with a relative density of Dr = 43.36%) and plane strain surface footings under static loading circumstances is imperative.

Therefore, the PIV experiments are intended to reveal failure patterns and displacement scales inside the gypseous sand, in addition to quantifying displacement fields and validating the outputs of the FEM model. The research attempts to provide a thorough understanding of soil behavior under loads by combining data from both methods, which will result in more dependable design solutions for foundations built on gypseous soils. This comprehensive study is expected to improve the engineering practices of current foundations, leading to increased safety and performance in regions vulnerable to gypseous soil issues.

2. MATERIAL AND EXPERIMENTAL METHODS

2.1 Material and Experimental Setup

The samples used here are gypseous sand deposits obtained from Fallujah City in Anbar Governorate, western Iraq. The properties of the sand were characterised for traditional tests using ASTM at Andrea Engineering Tests Laboratory **(Head, 1980; Jahanger et al., 2021)** according to previous **Tables 1 and 2** that refers to **(Jawad and Jahanger, 2024)**.

The following were the experimentally determined properties of the material: ($\gamma_{dmax.}$) = 16.93 kN/m^3; (γ_{dmin}) = 12.53 kN/m^3. Additionally, we used sieve analysis and the grain size distribution curve to determine the following characteristics of sand: D_{10} = 0.075 mm; D_{30} = 0.35 mm; D_{60} = 0.60 mm (10, 30, and 60% of the particles are smaller than the sizes shown); D_{50} = 0.31 (average size of soil particles); C_U = 6.670; and C_C = 3.26. Based on these numbers, it is noted that the soil is poorly graded silty sand SP-SM **(Liu and Iskander, 2004; Dijkstra et al., 2013)**. Furthermore, a standard compaction test was conducted in compliance with the specification **(ASTM D698, 2021)** to determine the highest dry density by **(Zbar et al., 2013)**, from which they calculated the following near densities in various ratios: 100% (16.93 kN/m^3), 90% (15.92 kN/m^3), and 80% (15.7 kN/m^3). Also, determined the field density (14.1 kN/m^3), which was verified to determine the density utilized in the test sample. Furthermore, the following Eq. (1) **(Shalaby, 2017)** is used to calculate the collapse index of the samples after the **(ASTM D5333, 1996)** method is followed utilizing single collapse and double odometer tests:

$$Cp(\%) = \frac{\Delta H}{H_0} = \frac{\Delta e_0}{1+e_0} \quad (1)$$

(Jennings and Knight, 1975) summarized severity of the collapse states as the inability to collapse when Cp is less than 1%, medium (between 1% and 5%), high (between 5 and 10%), very high (between 10% and 20%), and highly collapsible (more than 20%) **(Seleam, 2006)**. Furthermore, studies were carried out using the 'Digital Particle Image Velocimetry' (DPIV) program. As illustrated in **Fig. 1**, the model box was made an iron with inside dimensions of 700 mm × 700 mm × 700 mm was built to satisfy the optical and mechanical requirements. As a result, the model box was divided using an anti-oxidation paint-coated iron spacer that was length, 75 mm in width, 700 mm in height, and 10 mm in thickness. The front of the box is covered with a reinforced glass sheet that is 15 mm thick. This covering serves to both ensure the structural integrity of the box and ease testing by making the failure mechanism and sliding surface visible. Making sure the granular box can resist external forces under the ultimate load and minimize out-of-plane deformation of the walls (particularly the front measuring side) is crucial **(Jahanger et al., 2018a and 2018b; Cui et al., 2021)**. To lessen the impact of parameters on grain-scale displacements during DPIV experimental measures, the remaining portion of the box was constructed from smooth steel plates that were roughly 5 mm thick. Furthermore, this was confirmed using a dial gauge (precision of 0.01 mm) fastened to the side walls of a magnetic base (the picture of this setup is not shown here).

For this investigation, a 50 mm wide by 74 mm long by 25 mm thick steel foundation was created. It was the length of the foundation that is roughly equivalent to the 75 mm width of the separator tank, also the basis was somewhat rough according to **(Antony and Jahanger, 2020).** Based on available data, the angle of interfacial friction between the solid base and the gypseous sand exhibits a correlation of 0.6–0.7 **(Galavi et al., 2013)**. The sand grains' B/D_{50}>100 and the footing's varied dimensions combined to produce a side effect are lessened by the permissible range, which is represented by the ratio of 161 between the footing width (B) and average particle size (D_{50}) according to **(White et al., 2003; Dijkstra et al., 2013; Jahanger et al., 2018a and 2018b)**. In consideration of the aforementioned, a gap of 1 mm was established between the rear of the footing and the iron separator plate to decrease the impact of frictional forces.

The front of the box is used to make PIV measurements. It was ensured during testing that there was no significant grain loss through this gap. The footing model's base is forced into the top of the sand packing while the level, sand-filled box remains stationary. **Fig. 1** depicts

the entire footing test setup used in this experiment. It places a high-speed Nikon D7500 Digital SLR camera in front of the glass side of the box model. The resolution of the camera was 21 megapixels.

This method examines the bearing capacity of the model-scale footing and the deformation patterns of gypseous sandy soil under different loading conditions. This could improve our understanding of the behavior of gypseous soils, allowing us to design more effective engineering solutions for structures constructed on or inside these soils (gypseous sand soils).

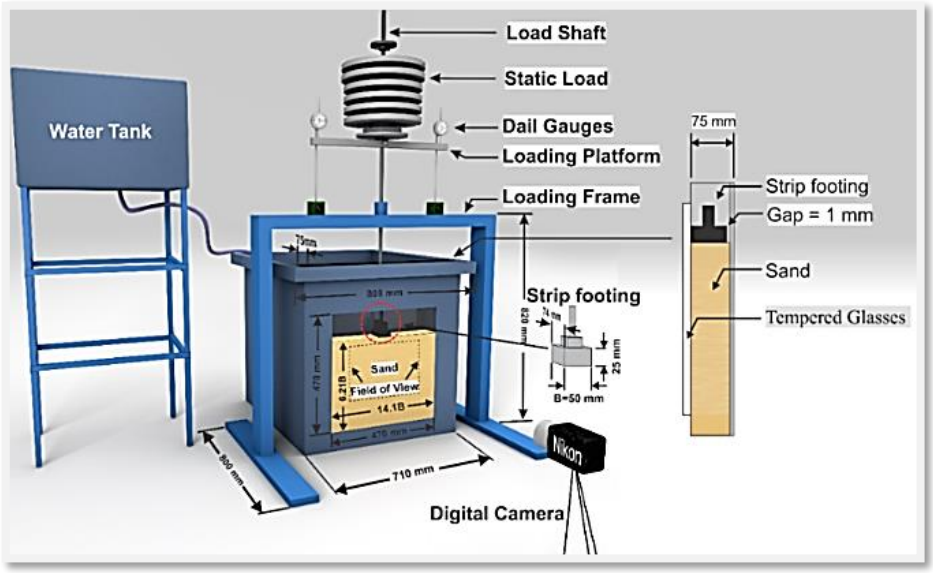

Figure 1. The experimental setup's schematic diagram using PIV with the high-speed camera (dimensions are in mm).

The displacement and velocity fields of tracer particles in the soil sample were analyzed using PIV software **(Fernández et al., 2021)**. The displacement field was calculated using Eq. (2) **(Atkins, 2016)**.

$$u = \frac{\Delta x}{\Delta t} \tag{2}$$

Where u is the displacement field in the x-direction Δx is the change in particle position, and Δt is the change in time. The velocity field in y-direction calculated using the Eq. (3):

$$v = \frac{\Delta u}{\Delta t} \tag{3}$$

Where v is the velocity field, Δu is the change in displacement, and Δt is the change in time. Terzaghi's Eq. (4) expresses the ultimate load-bearing capacity of a surface strip footing under the influence of homogeneous granular soil and a centrally applied vertical load **(Terzaghi, 1943)**:

$$q_u = \frac{1}{2}\gamma B\, N_\gamma \tag{4}$$

2.2 Preparation of Soil into Container

The sand was used for relative density Dr = 43.36% **(ASTM C128, 2012)**. First, the test box was filled with a filter layer of 75 mm coarse sand at the base to ensure that the soil mass was evenly moistened. Also, sand was poured steadily into the box using the falling pouring technique **(Jahanger et al., 2018a and 2018b; Ekbote and Nainegali, 2019),** forming three layers 100 mm thick on top of each other. A load-bearing column was used mounted on the base, with a weight not exceeding 5 kg, with an average of 15 strokes per layer, and it was specially made for gently compressed sand layers. It was used to compact each layer of sand to be suitable for what was required (sand height and packing density). Then a hand scraper for leveling the top surface of the sanding layer was used. The resulting compressed sand was allowed to settle for 24 hours and has a porosity of 0.40 **(Fattah et al., 2013)**. The sandbox was prepared as shown in **Fig. 1**, and the foundation was placed on the layer of compressed sand symmetrically with the rest of the parts shown in the figure. Finally, a camera was used and installed at a distance of approximately 150 cm to prevent vibrations.

2.3 Footing-Gypseous Sand Interactions Using PIV

The test and measurement were carried out for the probabilities of collapse (Cp) and associated settlement (Su), which are related to the static load experiments, and a study of facilitating the mechanical response between both the sand and the footing, where the static load was added during each hour, one after the other, and according to the sequence, the consolidation loads 25, 50, 100, and 200 kPa, during loading, and a loading column was used by applying a light axial compressive force to the base, The testing showed how the footing's load settled on the medium-dense sand, Where weight was applied until the sample's stress reached 200 kPa, as specified by **(ASTM D5333, 1996; Zhang et al., 2018)**. For the pressure to reach 200, weight was applied to the sample every hour, and pictures were taken every 10 seconds. This test was done in dry conditions, and then the water level was raised in a tank separate from the sandbox. Meanwhile, pictures were taken every ten seconds until the soil was saturated and after 24 hours had passed, as shown in **Fig. 1**. Also, take pictures for an hour. Noting that the two dial scales (0.01 mm/div for maximum 50 mm travel) are used throughout the test period. Though this might be minimized, it is known that the footing model's scale effects could alter the strength estimates **(Jahanger et al., 2018a and 2018b).** The findings of tests with studies utilizing laboratory models and the prototype may differ, even though small-scale models are frequently used to investigate how the full-size foundation operates in real life **(Vesić, 1973).**

2.4 PIV Analysis: Digital Particle Image Velocity

The digital instrument known as DPIV employs particle image velocimetry for PIV research. Tracer particles are frequently employed in the study of fluid mechanics to detect the velocity of particles within a fluid flow **(Schröder and Schanz, 2023)**. Displacement and strain distribution of granular packaging subjected to variable loads have been investigated by researchers utilizing DPIV **(O'Loughlin and Lehane, 2010; Hamm et al., 2011; Murthy et al., 2012; Jahanger and Antony, 2017; Jahanger et al., 2018a and 2018b)**. The fact that such an analysis for a static load on gypseous sandy soil was never published before is something that this study looks at. Whereas the DPIV analysis settings in this work were carefully made to allow accurate, high-resolution measures of the velocity fields in the sand packing under static stress.

For each succeeding load, the program PIV was supplied with an image every 10 seconds for an hour on the initial day to calculate the amount of soil displacement. Nonetheless, the following day, a photograph was captured every 10 seconds, 24 hours after the model was loaded with 200 kPa under dry conditions. The next day, after completing the saturation state, pictures were also taken every ten seconds for an hour, and after completing the test, where the images are separated into sets; the initial and final set images are disregarded to guarantee that the remaining set images exhibit the smallest possible nose during the on-and-off transitions of the camera, respectively.

In this study, the DPIV camera lens was usually focused on the 260 mm by 460 mm plane of the footing structure-soil interface area. **Fig. 2** shows the soil becoming deformed under static loading conditions. This made it possible to track individual soil particles. Since PIV is an optical method that doesn't change the medium, it can be used to find the flow fields of both fluid and particle media. Some of the things that affect how accurate and good the velocity readings are the size of the picture, the resolution of the pixels, and the rate at which the frames are taken. The image size was 5600 by 3700 pixels so that the whole footprint of the footing model would be recorded in each frame. To improve the accuracy of the displacement readings, a high pixel resolution of 21.41 by 8.06 pixels/mm was used. With a frame rate of 30 Hz (assuming the program uses 10 seconds), it was possible to catch the fast, dynamic processes that happen during static loading. Cross-correlation was used in the study to separate the velocity vectors and the motion fields. Whereas PIV made it possible to do a full analysis of how the soil collapsed. This included finding areas with high strain rates and describing how the patterns of deformation changed over time. Also, **(Ganju et al., 2020)** used PIV to look at how sandy soil changes when it is loaded steadily. The study found that PIV could accurately measure soil displacement fields, which made it possible to look closely at the deformation process. Technology keeps probing the sand particles in ever-smaller places to keep track of their movement. The particle photos used in this experiment worked best with a 64-by-64-pixel interrogation area. So, the measures of PIV experiments done here are on a small scale.

Figure 2. Image of photogrammetric target.

2.5 Finite Element Analysis

2.5.1 General

Plaxis 3D is a finite element package **(Brinkgreve and Vermeer, 1998)** made for analyzing deformation and stability in geotechnical engineering situations. Plaxis can handle several geotechnical issues, including slopes, retaining walls, tunnels, earth structures, and deep excavations. In a three-dimensional nonlinear finite element program, plain strain conditions are assumed, and a strip foundation under a constant load is modeled **(Raee et al., 2019)**. It was determined how effective the model was. In terms of width, the model footing is believed to extend four and a half times from each side on gypseous sandy soil. With the footing width B = 50 mm, t = 25 mm, and height = 300 mm, as indicated in **Fig. 3a,** the model geometry and fine meshing of the strip-footing system were created to match the lab model. The plane part divided in the tank was used to build the model. The degree to which the normalized scale displacements of gypseous sand media accord with the experimentally measured displacement pattern of the gypseous sand grains in footing-gypseous sand interactions, for example, when utilizing PIV as in this work—is also unclear. Therefore, the features of gypseous sand were put into the model so that they matched the lab sample **Table 3**. In this work, FEM simulations are used to look into this part of the problem as well as **Fig. 3 b**, which shows the geometry and mesh of the footing problem.

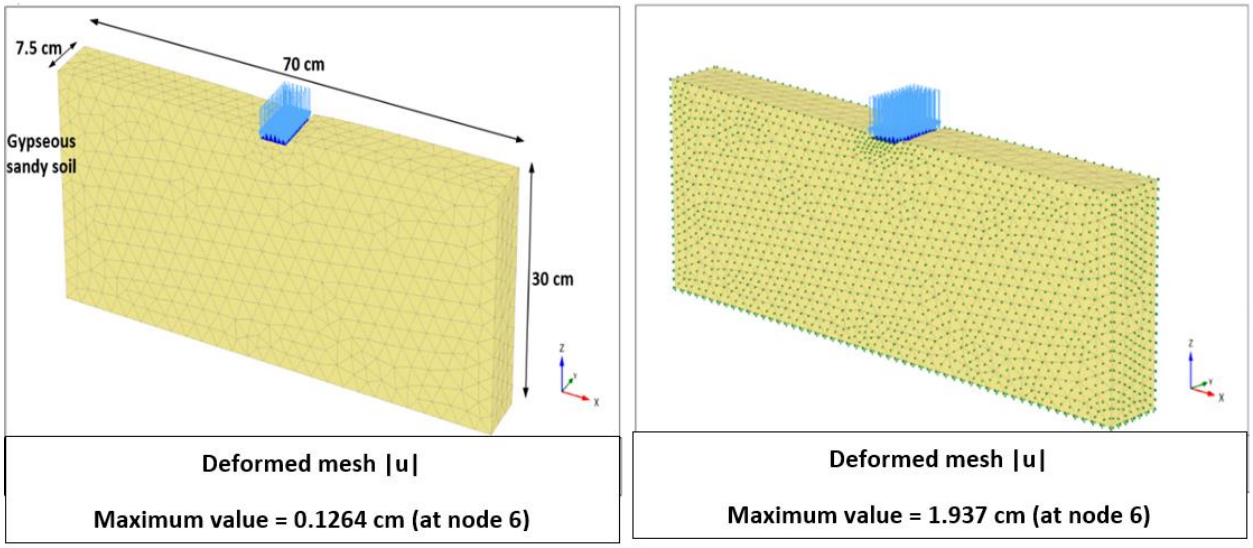

(a) (b)

Figure 3. (a) The geometry and meshing for footing width testing with B = 50 mm; (b) shows the schematic representation of the problem with the elements listed.

2.5.2 Finite-Element Modelling

To simulate the nonlinear behavior of gypseous sand, the linear, perfectly elastic Mohr-Coulomb model was applied. It was hypothesized that the sand layer had proper plane dimensions, and the depth was represented in the Plaxis model by using the drilling option. Table 3 provides a full breakdown of the parameters used in numerical study. For soil, it was considered to be dry, and for plate elements, it was believed to be non-porous. The impact of constitutive soil model type on behavior prediction was not investigated in this study; nevertheless, **(Durrani et al., 2006)** have validated the model's suitability. For a displacement of strip footing, the granular soil model was selected because confining

pressure causes an increase in the stiffness of strip footing, which can be captured by this model. Whereas Young's modulus was a role in evaluating the elastic behavior under applied pressure when analyzing analyzing gypseous sand soil and its interaction with strip footings using Plaxis 3D, where **(Budhu, 2010)** states that the coefficient values are necessary to estimate stability because it affects the deformation properties of the soil. Furthermore, the foundation's surface is subjected to a vertical load. The loading point of the soil model is selected for the analysis. Non-linear plasticity problems can be tackled with a variety of techniques offered by Plaxis 3D. The automatic selection of step size is the foundation of all procedures. One of the procedures is the loading sequence up to the maximum capacity. Generally speaking, the automatic step size process is used in phases of calculations where achieving a particular ultimate load level is necessary. Calculation of the procedure is terminated upon the detection of soil failure or the attainment of the designated load level. User-specified values for the total load to be applied constitute a crucial characteristic of this calculation procedure. The force per area is the unit of input for distributed loads in Plaxis 3D. Utilizing total load multipliers, the external load is ascertained on a global scale. Assuming no earlier collapse mechanism or discharging transpires. To ascertain the ultimate applied load subsequent to the calculation phase, the input load value is multiplied by the corresponding total load multiplier. In addition, the 3D finite element mesh comprises significant components such as a quantity of soil elements and 10-node tetrahedral elements.

Table 3. Input parameters for plane strain condition of the FEM program

Parameters	gypseous sandy soil	strip footing
Material model	Mohr-Coulomb	Linear Elastic
Material behavior	Drained	Elastic
Unit weight unsaturated, γ_{unsat}, kN/m^3	14.1	78.5
Unit weight saturated, γ_{sat}, kN/m^3	18.2	_
Young's modulus, E, kN/m^2	15000	200.0E6
Poisson's ratio, ν	0.30	0.26
Cohesion, c, kN/m^2	10	_
Friction angle,ϕ in dry	35.7°	_
Ditalatancy angle, ψ	0.9	_

3. RESULTS AND DISCUSSION

In this section, a summary of the test results of the model is presented with a discussion highlighting the effects of the different criteria. Showing all result numbers would have lengthened the paper, so only a selection is presented. Among the most important of these results, which were tested below:

3.1 Comparison of Laboratory Model Tests with Plaxis Load-Settlement Curves

Single and double odometer collapse test results (Cp) of 5.217% and (Cp) of 4.72%, respectively. These results of the field density of 14.1 kN/m^2 in the lab are shown in **Fig. 4.** Also, single collapse and double-odometer-tests were conducted for different densities at maximum dry density: 100% of maximum dry density, 90% of maximum dry density, and 80% of maximum dry density. It was concluded that the probability of collapse decreases with an increase in density and a decrease in the void ratio. The maximum collapse potential

in the laboratory was measured at the lowest density (field) adopted for the model test. The load-settlement relationship for a typical hard piece of gypseous sand is then displayed in **Fig. 5**, and it was discovered by subjecting the sample to loads of 25, 50, 100, and 200 kPa. Moreover, **Fig. 5** illustrates that the footing ultimate vertical settlement (Sv) to beam width (B) ratio (Sv/B) is 40.24% under soaking conditions for 24 hours and 3.56% under dry conditions. In contrast to Plaxis 3D, Sv/B is 2.49% and 38.41% in dry and soaking circumstances, respectively, which may be congruent with the lab model soil. Where collapse potential was 6.11% when conducting soil model test and applying it according to Equation (1) in Section (2.1). In this case, the permitted range of High collapsibility (5–10%) was reached by determining the soil condition and inclination to collapse as a first step in determining the severity of the collapse. Moreover, the elastically compressed area under the base is highly collapsible. Furthermore, under unsaturated 200 kPa loading circumstances, the soil has a low compressibility. Although the soil density was used similarly, the results obtained during this study provide insight into the differences between the model test (plane strain) and the odometer test (single-dimensional compression). The error percentage between a single-dimensional compression and an experimental test was found to be 0.85%.

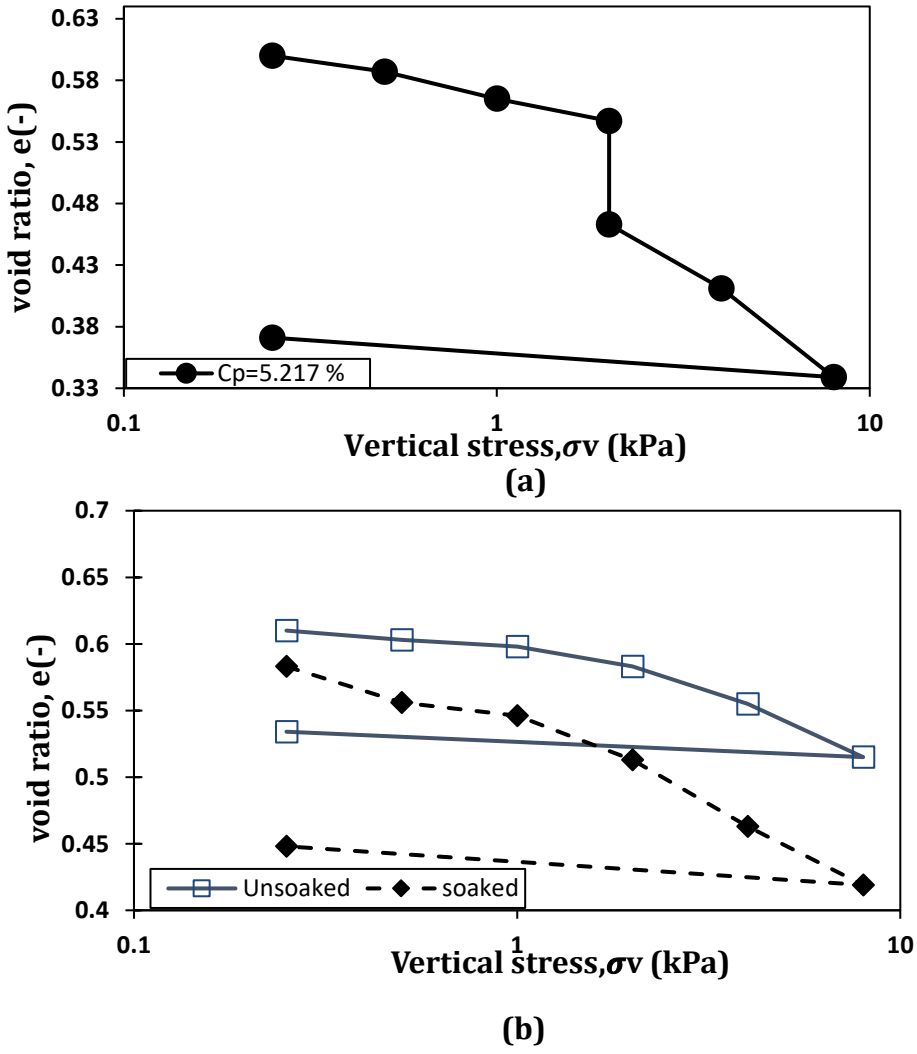

Figure 4. Collapse test includes a) a single collapse test and b) a double odometer test on reconstituted gypseous-sandy soils.

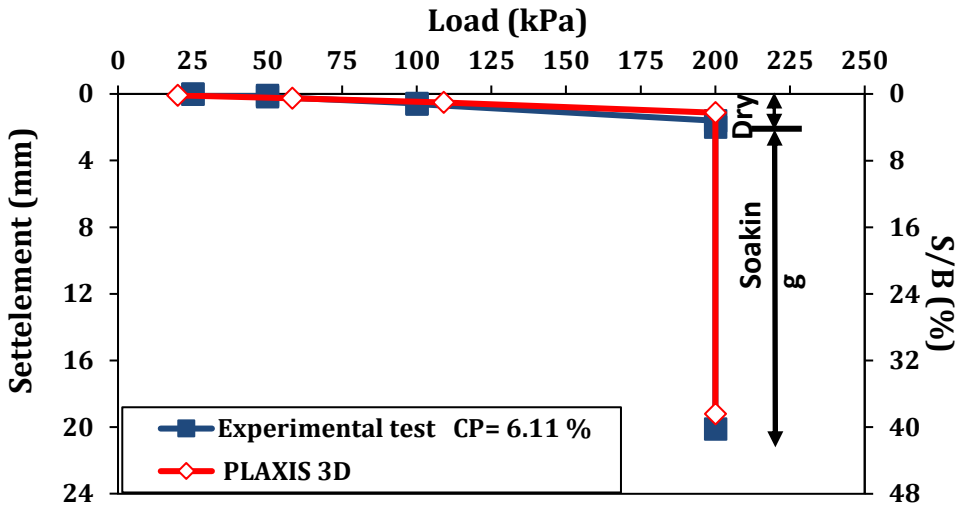

Figure 5. The load-settlement curve concerning strip footings on medium-dense gypseous sand.

3.2 Mean Resultant Vertical Displacement Vector Fields Gypseous Sandy Soil

The mean resultant displacement under the ultimate load measured using PIV-based methods is shown, along with the direction in which they are. As depicted in **Fig. 6**, soil deformation was primarily a vertical consolidation of the gypseous granular soil subsequent to system saturation from the bottom up. The experiment involves visually representing the magnitudes (represented by colored plots) and vectors of the incremental displacements in the time steps spanning from 24 hours of dry conditions to 24 hours of soaking. This enables a clear illustration of the vertical soil movement. This was clearly indicated **(Jawad and Jahanger, 2024)** in the results of the previous analysis of the program PIV through the analysis of the soil speed and after comparison with the failure **(Prandtl, 1920)** it was found that the type of failure is punching shear failure due to the vertical displacement movement and speed downward. This results when exposing the sandy gypsum soil to static loads ranging from 25 to 200 kPa under drought and soaking conditions altered the homogeneous deformation pattern. When saturated with water, gypseous soil is susceptible to abrupt collapse **(Al-Saoudi et al., 2013)**. Where note softening of gypsum materials situated between the soil's particulates transpire in the event of a rising water table, which may be caused by various factors. This condition results in the disruption of the interparticle bonds formed by the gypsum materials with the soil **(Husain et al., 2018; Abdalhusein and Ali Akhtarpour, 2019)**. The panels, however, display the outcomes pertaining to a specific category of static load wherein the vertical and horizontal displacements' scalar contours are superimposed on the displacement vector maps that are produced, as seen in **Fig 6**. This picture illustrates whether soil displacements in a horizontal or vertical direction are responsible for the failure process in gypseous sand media under a static load. It is noteworthy to mention that water infiltration into the supporting gypseous soils may result in structural damage and cracking **(Ahmed, 2013; Fernandes et al., 2015)**. This procedure generates a "meta-stable" structure that facilitates the sliding of particles into a denser state. The progressive partial rupture of the gypseous sandy soils during the loading process can be attributed to this factor, as its relative density accounted for 43.36% of the total density of the type (medium-dense to loose sand). Due to compaction, the soil friction angle is

therefore greater for loose sand at failure than it was at the onset of loading. Contrarily, this does not apply to dense sand. Therefore, medium-dense gypseous sand supports the foundation collapse as depicted in **Fig. 6**, which may be examined using the PIV program.

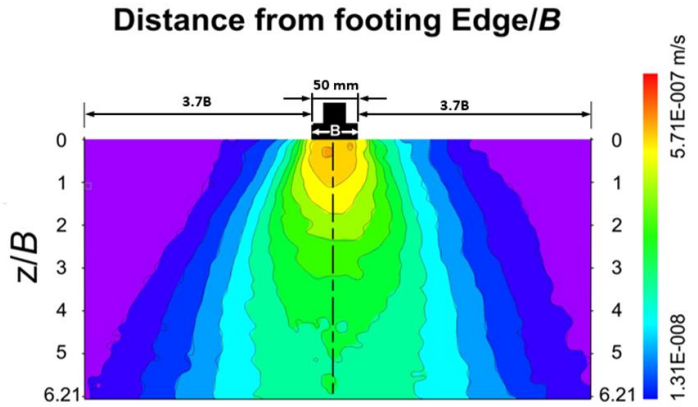

Figure 6. Scalar map of the mean displacement that results from using PIV on field gypseous sandy soil under a stress level of 200 kPa.

In addition, as **Fig. 7** illustrates, the outcomes of the initial test are reasonably similar to those taken into account in various loading stages in Plaxis analysis. **Figs. 6 and 7** also show the comparison of incremental displacements in numerical and laboratory samples. There is good agreement in the outcomes that were obtained. The slight discrepancy in quality, aside from the estimations of computer modeling, could be attributed to the lighting conditions in the laboratory and the corresponding errors in PIV analysis. Moreover, there are a few discrepancies in the displacements produced by numerical simulation and those determined by PIV. To detect incremental soil displacement indirectly, particle image velocimetry was used. A moving and deforming soil sample's incremental displacement field is computed from two consecutive photographs. They are recorded in different loading phases that are similar to, but different from, those considered in different loading stages of the Plaxis analysis. The maximal displacements in the PIV analysis are, therefore, greater than those in the Plaxis analysis. In addition, the material behavior models that have been incorporated into Plaxis are oversimplified depictions of the actual behavior of soil and strip foundations **(Raee et al., 2019)**.

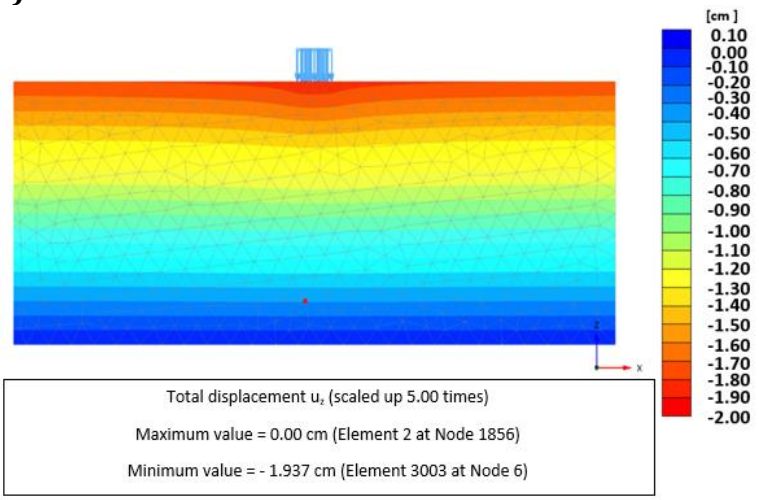

Figure 7. Shows the saturated gypseous resultant vertical displacement below the footing.

3.3 Vorticity Profiles

PIV provides two-dimensional, velocity field data that are spatially defined and have a resolution high enough to estimate the out-of-plane component of the vortex **(Gurka et al., 2006)**. The PIV looked at the gypseous soil collapse pattern depicted in **Fig 8**. The objective is to determine the key elements that are related to entropy and deformation in the turbulent flow of gypseous sand soaking. The results for the test showed a similar pattern of increasing vortice readings with increasing load and elapsed time. However, the readings were slightly different, likely due to variations in the soil sample or testing conditions. Overall, these results suggest that both the applied load and the elapsed time have a significant impact on the vortices of the gypseous soil under collapse loading conditions, with higher loads and longer durations resulting in greater vortices. Additionally, the soil conditions (dry or soaking) also appear to have a notable impact on the vortices readings, with soaking conditions generally resulting in higher vortices. This observation provides valuable insights into the collapse pattern of gypseous soil and highlights the importance of understanding the soil's behavior and distribution under static load scenarios.

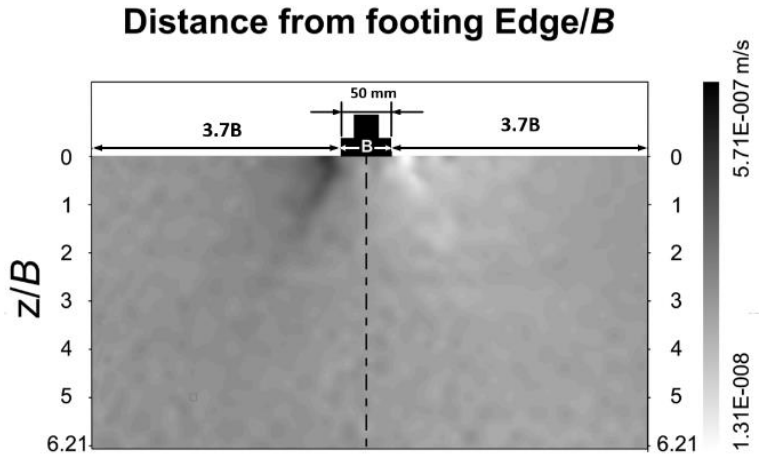

Figure 8. The vorticity resultant of displacement on field gypseous sandy soil using PIV at a stress level of 200 kPa

3.4 Maximum Shear Strain Rate Distribution Across the Ultimate Load

To find out how much gypsum soils vary when loads are applied at different times, we measured the du/dx and dv/dy strain rates in our experiment using PIV. The development of small, highly deformed zones where particles underwent significant shear strains was another feature of localized shear bands. In **Fig. 9**, the failure envelope of gypseous under collapse loading circumstances is examined by taking the highest shear strain rate fields from the displacement fields. Consequently, temperature, permeability, flow conditions, and environmental changes in moisture content resulting from variations in the groundwater table and/or surface water, gypsum type and quantity, and gypsum type and quantity all influence the rate of gypsum dissolution. During the last 30 years, there have been a lot of efforts in Iraq to study and understand how gypseous soils behave in different environments and under various loads **(Zedan and Abbas, 2020)**. This was done through intense research programs at many institutions. Numerical methods were also used to model the process of gypsum dissolving when it was soaked and leached. Due to the complexity of the gypseous soils, the large amounts of data from the long-term study programs often showed results that

were at odds with each other. So, no firm decisions have been made yet. The PIV software was focused on the collapsibility and deformability of sandy gypsum soil. The behavior of granular materials can be reliably investigated using PIV, a non-intrusive technology, but it is important to take into account its limitations and the impacts of the experimental apparatus's scale. This was deemed to be utilizing a plane box with dimensions more significant than the footing model in the current study. More research is needed to fully understand the limitations and scale implications of the PIV while analyzing the behavior of granular materials under different loading scenarios. In order to gain an understanding of the collapse patterns, PIV was therefore utilized to study the deformation behavior of gypseous soils. For the entire cartesian strain, saturated gypseous sandy soil was also simulated using the Plaxis program, as seen in **Fig. 10**.

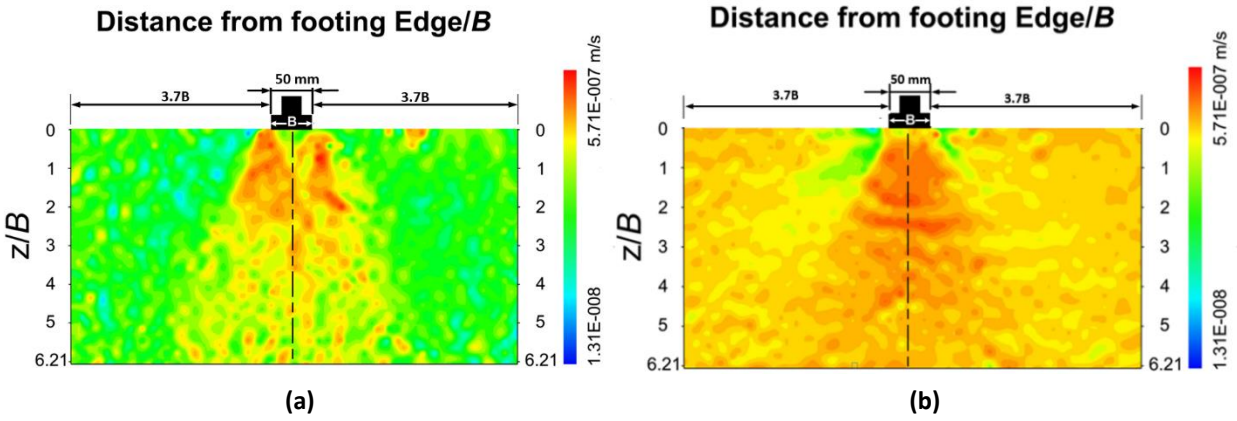

Figure 9. Behavior of Natural Soil Under 200 kPa Load: (a) horizontal displacement du/dx, (s^{-1}), and (b) vertical displacement dv/dy, (s^{-1}),

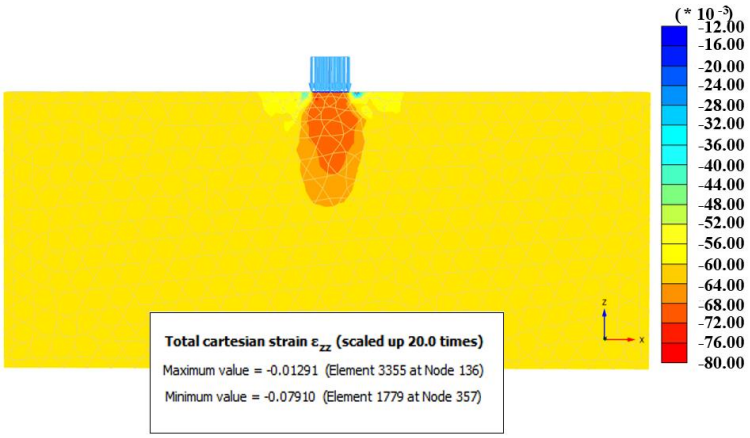

Figure 10. Total cartesian strain for saturated gypseous sandy soil under 200kPa final load.

4. CONCLUSIONS

The Particle Image Velocimetry was a potent instrument for comprehending the geotechnical characteristics of footings embedded in gypseous sand. The results indicate a strong correlation between experimental displacement measurements and velocity profiles, which is consistent with previous research and finite element method (FEM) analyses. PIV effectively captures the nuanced stages of velocity discontinuities within the sand, showcasing its ability to visualize displacement patterns under static loading conditions. In the PIV analysis, we identified a specific failure zone that was the consequence of the soil's

downward movement and tilting over the foundation distances. The punching shear failure that we found in this analysis is considered one of the main types of failure, which is referred to as shallow failure resulting from the collapse patterns of field gypseous sand soils with regular concavities, and the patch size of the PIV analysis for normal condition tests was 21.41 × 8.06 pixels/mm. In addition, the experimental results and the numerical model results demonstrate a strong accord in the overall load-settlement pattern that defines the deformation of the strip foundation. Variations in the soil parameter, experimental mistakes, or model-induced variations are usually invariably the cause of discrepancies between the value acquired from strip-footing model tests and the collapse pattern determined using FEM.

NOMENCLATURE

Symbol	Description	Symbol	Description
γ_{dmax}	Maximum Dry Density	e_o	Void ratio at field packings.
γ_{dmin}	Minimum Dry Density	E	Young's modulus
γ_{dfield}	Field Dry Density	ν	Poisson's ratio
du/dx	Horizontal displacement	Δe	Void ratio changes by the wetting process.
dv/dy	Vertical displacement	D_{10}	The diameter corresponding to the passing percentage of 10% of the soil sample
Dr	Relative Density	D_{30}	The diameter corresponding to the passing percentage of 30% of the soil sample
ΔH	Height changes by the wetting process.	D_{60}	The diameter corresponding to the passing percentage of 60% of the soil sample
H_o	Sample height at the initial state	D_{50}	Average Grain Size Diameter
C	Cohesion	Cu	Coefficient of uniformity
Sv/B	Ultimate vertical settlement (Sv) to beam width (B) ratio	Cc	Coefficient of gradation
Cp	Collapse Potential	SP-SM	Poorly graded silty sand
B	Width	t	Thickness
FEM	Finite Element Method	PIV	Particle Image Velocimetry
ϕ	Friction angle,ϕ in dry	ψ	Ditalatancy angle, ψ

Acknowledgements

The authors acknowledge Dr. S. J. Antony, University of Leeds, for using PIV software.

Credit Authorship Contribution Statement

Hala Mahmood Jawad: Conceptualization, Investigation, Software, and Validation
Zuhair Kadhim Jahanger: Conceptualization, Review & editing, Methodology, and Validation

Declaration of Competing Interest

The authors declare that they have no known competing financial interests or personal relationships that could have appeared to influence the work reported in this paper.

REFERENCES

Abd-Alhameed, H.J. and Al-Busoda, B.S., 2023. Experimental study on the behavior of square-skirted foundation rested on gypseous soil under inclined load. *Journal of Engineering,* 29(03), pp.27-39. https://doi.org/10.31026/j.eng.2023.03.03.

Abdalhusein, M.M., Ali Akhtarpour, M.S.M., 2019. Effect of wetting process with presence of matric suction on unsaturated gypseous sand soils. *Journal of Southwest Jiaotong University,* 54(5).

AbdulRahman, S., Fattah, M.Y. and Ihsan, E.A., 2021. Influence of plastic fiber on the geotechnical properties of gypseous soil. *International Journal of Engineering,* 34(2), pp.367-374. https://doi.org/10.5829/ije.2021.34.02b.08.

Adrian, R.J., 1991. Particle-imaging techniques for experimental fluid mechanics. *Annual Review of Fluid Mechanics*, 23(1), pp.261-304.

Ahmad, F., Said, M.A. and Najah, L., 2012. Effect of leaching and gypsum content on properties of gypseous soil. *International Journal of Scientific and Research Publications,* 2(9), pp.1-5.

Ahmed, K.I., 2013. Effect of Gypsum on the Hydro-Mechanical Characteristics of Partially Saturated Sandy Soil. Doctoral dissertation, Cardiff University. https://orca.cardiff.ac.uk/id/eprint/58191.

Alimardani Lavasan, A., Ghazavi, M., 2014. Failure mechanism and soil deformation pattern of soil beneath interfering square footings. *Numerical Methods in Civil Engineering,* 1(2), pp.48-56. https://doi.org/10.29252/nmce.1.2.48.

Al-Mufty, A.A., 1997. Effect of gypsum dissolution on the mechanical behaviour of gypseous soils. Unpubl (Doctoral dissertation, Ph.D. Thesis, Department of Civil Engineering. Baghdad, Baghdad, Iraq).

Al-Obaidi, Q.A., Mohsen, M.K. and Asker, A.O., 2022. Investigation of the bearing capacity and collapsibility of gypseous soil using geotextile reinforcement. *Engineering and Technology Journal,* 40(05), pp.792-801. https://www.iasj.net/iasj/download/f08dd3917d8f679e.

Al-Saoudi, N.K., Al-Khafaji, A.N. and Al-Mosawi, M.J., 2013. Challenging problems of gypseous soils in Iraq. *In Proceedings of the 18th International Conference on Soil Mechanics and Geotechnical Engineering,* pp. 479-482. https://www.cfms-sols.org/sites/default/files/Actes/479-482.pdf.

Antony, S.J. and Jahanger, Z.K., 2020. Local scale displacement fields in grains–structure interactions under cyclic loading: Experiments and simulations. *Geotechnical and Geological Engineering,* 38(2), pp.1277-1294. https://link.springer.com/article/10.1007/s10706-019-01088-5.

ASTM C128, 2012. Standard Test Method for Density, Relative Density (Specific Gravity), and Absorption of Fine Aggregate. ASTM International, West Conshohocken, PA. https://www.astm.org/c0128-12.html.

ASTM D5333, 1996. Standard test method for measurement of collapse potential of soils. The American Society for Testing and Materials, USA. https://www.astm.org/d5333-03.html.

ASTM D698, 12021. Standard Test Methods for Laboratory Compaction Characteristics of Soil Using Standard Effort. The American Society for Testing and Materials, USA. https://www.astm.org/d0698-12r21.html.

Atkins, M.D., 2016. Velocity Field Measurement Using Particle Image Velocimetry (PIV). *In Application of thermo-fluidic measurement techniques,* pp. 125-166. https://doi.org/10.1016/B978-0-12-809731-1.00005-8.

Brinkgreve, R.B., and Vermeer, P.A., 1998. Plaxis Version 7.2 Manual, finite element code for soil and rock analyses. AA Balkema/Rotterdam/Brookfield, Rotterdam, The Netherlands.

Budhu, M., 2010. *Soil Mechanics and Foundations*. John Wiley and Sons.

Cui, M., Chen, F. and Bu, F., 2021. Multiphase theory of granular media and particle simulation method for projectile penetration in sand beds. *International Journal of Impact Engineering,* 157, p.103962. https://doi.org/10.1016/j.ijimpeng.2021.103962

Das, B.M., 2017. Bearing capacity and settlement. *Shallow foundations*: CRC press. https://doi.org/10.1201/9781315163871.

Dijkstra, J., Gaudin, C. and White, D.J., 2013. Comparison of failure modes below footings on carbonate and silica sands. *International journal of physical modelling in geotechnics,* 13(1), pp.1-12. https://doi.org/10.1680/ijpmg.12.00004.

Durrani, J.K., Ellis, E.A. and Reddish, D.J., 2006. Modelling lateral pile–soil interaction for a row of piles in a frictional soil. *In 4th international FLAC symposium numerical modelling geomech,* pp. 231-238.

Ekbote, A.G., Nainegali, L., 2019. Interference of two closely spaced strip footings embedded in cohesionless fibre-reinforced foundation soil bed. *In Eighth International Conference on Case Histories in Geotechnical Engineering*, pp. 454-464. https://doi.org/10.1061/9780784482094.041.

Fattah, M.Y., Ahmed, M.D. and Mohammed, H.A., 2013. Determination of the shear strength, permeability and soil water characteristic curve of unsaturated soils from Iraq. *Journal of Earth Sciences and Geotechnical Engineering,* 3(1), pp.97-118. https://www.scienpress.com/Upload/GEO/Vol%203_1_8.pdf.

Fernandes, N.L., Barreto, N.M.B., Machado, A.C. and Rocha, G.P., 2015. Comparative study between methodologies used for determination of the total hardness in aqueous matrices. *Periódico Tchê Química, 12(24),* pp.91-95. https://www.cabidigitallibrary.org/doi/full/10.5555/20153404927.

Fernández, M.E., Pugnaloni, L.A. and Sánchez, M., 2021. Proppant transport in a planar fracture: Particle image velocimetry. *Journal of Natural Gas Science and Engineering,* 89, p.103860. https://doi.org/10.1016/j.jngse.2021.103860.

Galavi, V., Petalas, A. and Brinkgreve, R.B.J., 2013. Finite element modelling of seismic liquefaction in soils. *Geotechnical Engineering Journal of the SEAGS & AGSSEA,* 44(3), pp.55-64.

Ganju, E., Han, F., Prezzi, M., Salgado, R. and Pereira, J.S., 2020. Quantification of displacement and particle crushing around a penetrometer tip. *Geoscience Frontiers,* 11(2), pp.389-399. https://doi.org/10.1016/j.gsf.2019.05.007.

Gurka, R., Liberzon, A. and Hetsroni, G., 2006. POD of vorticity fields: A method for spatial characterization of coherent structures. *International Journal of Heat and Fluid Flow,* 27(3), pp.416-423. https://doi.org/10.1016/j.ijheatfluidflow.2006.01.001.

Hamm, E., Tapia, F. and Melo, F., 2011. Dynamics of shear bands in a dense granular material forced by a slowly moving rigid body. *Physical Review E,* 84(4), p.041304. https://doi.org/10.1103/PhysRevE.84.041304.

Hassan, S.M., and Al-Busoda, B.S., 2023. Evaluation the behavior of ring footing on gypseous soil subjected to eccentric and inclined loads. *Journal of Engineering,* 29(5), pp.79-89. https://doi.org/10.31026/j.eng.2023.05.06.

Head, K.H., 1980. *Manual of soil laboratory testing (Vol. 1, No. 2).* London: Pentech press. http://dx.doi.org/10.1179/1938636213Z.00000000045.

Husain, M.M.A., Akhtarpour, A. and Mahmood, M.S., 2018. Wetting challenges on the gypsiferous soils. *In proceedings of the 4th International Conference on Civil Engineering, Architecture and Urban Planning.*

Jahanger, Z.K., Al-Barazanchi, A.J.N., and Ahmed, A.A., 2021. Field soil electrical resistivity measurements of some soil of Iraq. *Proceedings of the 6th GeoChina International Conference on Civil & Transportation Infrastructures: From Engineering to Smart & Green Life Cycle Solutions Nanchang, China,* 2021 6 (pp. 114-122). https://link.springer.com/chapter/10.1007/978-3-030-80155-7_8.

Jahanger, Z.K., and Antony, S.J., 2017. Application of digital particle image velocimetry in the analysis of scale effects in granular soil. *In International Scholarly and Scientific Research & Innovation,* Vol. 11, No. 7, pp. 910-915. https://eprints.whiterose.ac.uk/116866/.

Jahanger, Z.K., Antony, S.J., Martin, E., and Richter, L., 2018b. Interaction of a rigid beam resting on a strong granular layer overlying weak granular soil: Multi-methodological investigations. *Journal of Terramechanics,* 79, pp.23-32. https://doi.org/10.1016/j.jterra.2018.05.002.

Jahanger, Z.K., Sujatha, J., and Antony, S.J., 2018a. Local and global granular mechanical characteristics of grain–structure interactions. *Indian Geotechnical Journal,* 48(4), pp.753-767. https://link.springer.com/article/10.1007/s40098-018-0295-5.

Jawad, H.M., and Jahanger, Z.K., 2024. Collapse pattern in gypseous soil using particle image velocimetry. *In IOP Conference Series: Earth and Environmental Science (Vol. 1374, No. 1, p. 012012). IOP Publishing*. https://iopscience.iop.org/article/10.1088/1755-1315/1374/1/012012/meta.

Jennings, J.E., and Knight, K., 1975. A Guide to construction on or with materials exhibiting additional settlement due to collapse of grain structure.

Kuttah, D., and Sato, K., 2015. Review on the effect of gypsum content on soil behavior. *Transportation geotechnics*, 4, pp.28-37. https://doi.org/10.1016/j.trgeo.2015.06.003.

Liu, J., and Iskander, M., 2004. Adaptive cross correlation for imaging displacements in soils. *Journal of computing in civil engineering,* 18(1), pp.46-57. https://doi.org/10.1061/(ASCE)0887-3801(2004)18:1(46).

Mohsen, A.H., and Albusoda, B.S., 2022. The collapsible soil, types, mechanism, and identification: A review study. *Journal of Engineering,* 28(5), pp.41-60. https://doi.org/10.31026/j.eng.2022.05.04.

Murthy, T.G., Gnanamanickam, E., and Chandrasekar, S., 2012. Deformation field in indentation of a granular ensemble. *Physical Review E,* 85(6), p.061306. https://doi.org/10.1103/PhysRevE.85.061306.

O'Loughlin, C.D., Lehane, B.M., 2010. Nonlinear cone penetration test-based method for predicting footing settlements on sand. *Journal of geotechnical and geoenvironmental engineering,* 136(3), pp.409-416. https://doi.org/10.1061/(ASCE)GT.1943-5606.0000228.

Prandtl, L., 1920. On the Hardness of Plastic Bodies. Nachr. Gottinger Nachrichten, 74–85. (In German).

Punmia, B., and Jain, A.K., 2005. *Soil mechanics and foundations.* Firewall Media.

Raee, E., Hataf, N., Barkhordari, K., and Ghahramani, A., 2019. The effect of rigidity of reinforced stone columns on bearing capacity of strip footings on the stabilized slopes. *International Journal of Civil Engineering,* 17, pp.673-685. https://link.springer.com/article/10.1007/s40999-018-0291-2.

Schröder, A., and Schanz, D., 2023. 3D Lagrangian particle tracking in fluid mechanics. *Annual Review of Fluid Mechanics*, 55, pp.511-540. https://doi.org/10.1146/annurev-fluid-031822-041721.

Seleam, S.N., 2006. Evaluation of collapsibility of gypseous soils in Iraq. *Journal of Engineering*, 12(03), pp.712-726. https://doi.org/10.31026/j.eng.2006.03.21.

Shalaby, S.I., 2017. Potential collapse for sandy compacted soil during inundation. *International Journal Innovation Science Engineering Technology*, 4(5), pp.307-314. https://ijiset.com/vol4/v4s5/IJISET_V4_I05_47.pdf.

Terzaghi, K., 1943. Liner-plate tunnels on the Chicago (Il) subway. *Transactions of the American Society of Civil Engineers,* 108(1), pp.970-1007. https://doi.org/10.1061/TACEAT.0005664.

Vaughan, P.R., 2009. prediction and reality in geotechnical engineering. *In Selected papers on Geotechnical Engineering,* pp. 305-341. https://www.icevirtuallibrary.com/doi/abs/10.1680/spogebprv.36208.0016.

Vesić, A.S., 1973. Analysis of ultimate loads of shallow foundations. *Journal of the Soil Mechanics and Foundations Division,* 99(1), pp.45-73. https://doi.org/10.1061/JSFEAQ.0001846.

White, D.J., Take, W.A., and Bolton, M.D., 2003. Soil deformation measurement using particle image velocimetry (PIV) and photogrammetry. *Geotechnique*, 53(7), pp.619-631. https://doi.org/10.1680/geot.2003.53.7.619.

Zbar, B.S., Khan, M.A., and Jawad, A.S., 2013. Geotechnical properties of compacted silty clay mixed with different sludge contents. *In International conference for geotechnical engineering and transportation,* ICGTE (Vol. 31). https://www.iasj.net/iasj/download/0c93d2369a363da6.

Zedan, A.J., and Abbas, H.H., 2020. Experimental investigation of square footing resting on sand over gypseous soils. *Tikrit Journal of Engineering Sciences*, 27(1), pp.30-39. https://doi.org/10.25130/tjes.27.1.05.

Zhang, Y., Hu, Z., and Xue, Z., 2018. A new method of assessing the collapse sensitivity of loess. *Bulletin of Engineering Geology and the Environment*, 77, pp.1287-1298. https://link.springer.com/article/10.1007/s10064-018-1372-9.

مغلف الانهيار في التربة الرملية الجبسية باستخدام طريقة العناصر المحدودة وقياس سرعة الصورة الجزيئية

هاله محمود جواد[1]، زهير كاظم جهان كير[2]، *

[1] قسم الهندسة المدنية، كلية الهندسة، جامعة بغداد، بغداد، العراق
[2] قسم هندسة الموارد المائية، كلية الهندسة، جامعة بغداد، بغداد، العراق

الخلاصة

إن ارتفاع منسوب المياه وكذلك تسرب المياه إلى وسط التربة الجبسية يمكن أن يؤدي إلى خسارة كبيرة في حجم التربة، مع أو بدون إضافة الحمل. لم تتم دراسة السلوك الكلي الميكانيكي للتربة الرملية الجبسية باستخدام قياس سرعة الصور الجزيئية بعد، مع التركيز بشكل خاص على أنماط الانهيار. وقد حظيت هذه الأنماط الفريدة باهتمام الباحثين في التربة القابلة للتشوه، ولكن لا تزال هناك حاجة إلى معالجة صعوبات التربة الرملية الجبسية. وبالتالي، تهدف هذه الدراسة إلى تحديد مجالات الإزاحة على نطاق محلي وأنماط فشل الأساس الشريطي الصلب المتفاعل مع الرمل الجبسي تحت إجهاد ثابت قيد المقارنة، مع التركيز على الترطيب الناتج عن ارتفاع منسوب المياه والحالة الجافة باستخدام النموذج التجريبي وطريقة العناصر المحدودة. أظهرت نتائج قياس سرعة الصور الجزيئية أن نمط انهيار التربة الرملية الجبسية هو من نوع فشل القص الثاقب، مما أثبت صحة طريقة العناصر المحدودة وهذه الأنماط المتعلقة بالتشوه الرأسي للتربة. حيث كانت نتائج طريقة العناصر المحدودة وقياس سرعة الجسيمات متوافقة بشكل جيد. بالإضافة إلى ذلك، فإن نماذج التربة المبنية بطريقة العناصر المحدودة هي في الأساس تمثيلات مبسطة للغاية للسلوك الحقيقي للأساس. تكشف النتائج أن أنماط الفشل على نطاق محلي لوسط التربة الجبسية ضرورية لتحسين تصميم الأساسات

الكلمات المفتاحية: تربة جبسية، اساس شريطي، قياس سرعة صورة الجسيمات، طريقة العناصر المحدودة.